Dynamical behavior and peak power reduction in a pair of energy storage oscillators coupled by delayed power price

Tomohiro Fukunaga,[1] Tomoaki Imasaka,[1] Akira Ito,[2] Yoshiki Sugitani,[1] Keiji Konishi,[1] and Naoyuki Hara[1]
[1]*Department of Electrical and Information Systems, Osaka Prefecture University, 1–1 Gakuen-cho, Naka-ku, Sakai, Osaka 599-8531 Japan*
[2]*Engineering R&D Center, DENSO CORPORATION, 1-1 Showa-cho, Kariya, Aichi 448-8661 Japan*
(Received 18 November 2015; published 29 February 2016)

This paper investigates dynamics of a management system for controlling a pair of energy storages. The system involves the following two characteristics: each storage behaves in a manner that reduces the number of charge noncharge cycles and begins to be charged when the price of power is lower than a particular price threshold. The price is proportional to the past total power flow from a power grid to all storages. A peak of the total power flow occurs when these storages are charged simultaneously. From the viewpoint of nonlinear dynamics, the energy storages can be considered as relaxation oscillators coupled by a delay connection. Our analytical results suggest that the peak can be reduced by inducing an antiphase synchronization in coupled oscillators. We confirm these analytical results through numerical simulations. In addition, we numerically investigate the dynamical behavior in 10 storages and find that time delay in the connection is important in reducing the peak.

DOI: 10.1103/PhysRevE.93.022220

I. INTRODUCTION

Many interesting nonlinear phenomena can occur in multiple self-oscillations with mutual connections, even when there is no centralized control. Such phenomena have received considerable attention in nonlinear science [1–5] and are now used in a number of engineering applications, such as secure communication [6,7], control of robotics [8], sensor networks [9], antenna beam forming [10,11], frequency down converters [12,13], and parallel power converters [14,15].

Power-grid networks have been attracting increasing attention not only in the industrial arena but also in nonlinear science [16–19]. The smartgrid and microgrid concepts, which deal with the control of power-grid networks with distributed users and power sources, are expected to play an important role in future energy systems [20]. Energy storages are considered as essential for stable operation of power-grid networks [21]. In particular, it is well accepted that the management of distributed energy storages will be a key to the smart control of power-grid networks.

There have been many practical management schemes for controlling distributed energy storages, in which each such storage belongs to its own user (agent) (e.g., see Refs. [22–25]). These schemes must obtain all users' states and demands and then manipulate the users on the basis of the information obtained. These schemes involve the following problems: They have a heavy load of appropriate manipulations to compute for all users on the basis of the enormous amount of obtained information; the software for the computation must use complicated algorithm to accommodate a wide variety of changing situations, such as new user entry, old user exit, and system parameter change; and obtaining information and manipulating users require interactive communication [26]. Therefore, the initial cost of establishing an energy system including hardware and software and the cost of running the system would inevitably be high.

The reduction of peak load [27] has been recognized as one of the most important problems to be solved for power systems. To the authors' knowledge, however, there have been only a few attempts to utilize nonlinear phenomena in the power systems community. The present paper proposes a distributed system, a real-time power price systems, based on knowledge of nonlinear dynamics. This paper is concerned with the simple situation,[1] illustrated in Fig. 1, in which there are several users each of which possesses its own storage (e.g., electric battery or thermal storage) and purchases power from a common power grid (i.e., power source). Each user manipulates its own storage independently in accordance with the following two simple rules: (a) Each user aims to reduce the number of charge noncharge cycles to prevent storage degradation [28] and to reduce power loss in converting energy and (b) each user aims to purchase power for its own benefit when the price is less than a threshold. The common power price for all users is assumed to be proportional to the *past* total power flow. This is because a particular length of time is required to measure the total power flow and to inform the power price to every user [29–31].

In comparison with the most previous schemes, our system has the following features: Data required for communication is only the past total power flow (i.e., scalar data); there is no need to use interactive and high-speed communication, because past data are sent unidirectionally to all users; and the algorithm for control, rules (a) and (b), is quite simple. These features allow our system to take advantage of low initial and running costs.

It should be emphasized that energy storages with rules can be regarded as coupled oscillators, as illustrated in Fig. 2. As the energy state of each storage is self-oscillatory with slow and fast time scales, the storages behave as relaxation oscillators [32,33]. The storages are interacted via the common delayed power price which tends to push the energy state

[1]Practical situations in which there are various types of users and various energy sources are difficult to analyze. Thus, this article focuses on one of the simplest situations to analytically investigate the fundamental dynamics of storage users.

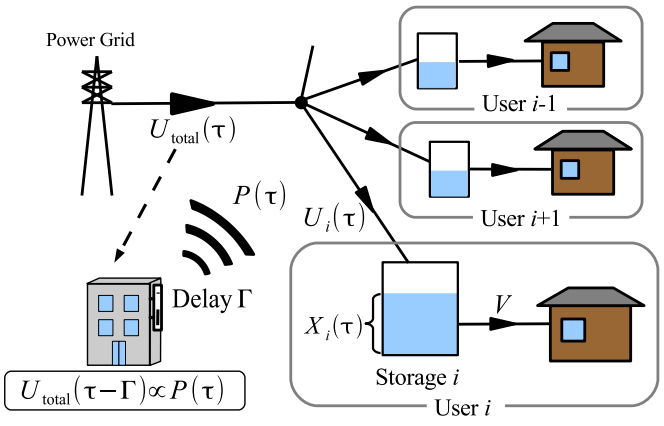

FIG. 1. Storages with delayed power price.

phases apart. Thus the interaction can be regarded as a repulsive connection with delay [34]. From the viewpoint of nonlinear science, the present paper investigates the dynamics of relaxation oscillators globally coupled by a repulsive delay connection and provides a procedure to design parameters inducing antiphase synchronization.

This paper analytically investigates the dynamical behavior of our system with a pair of storages from the viewpoint of nonlinear dynamics. The analytical results provide a condition for avoiding the peak load; moreover, this condition allows us to systematically design our system for peak load reduction. These analytical results and the design procedure are confirmed through numerical simulations. Furthermore, the dynamics of 10 storages is numerically investigated, and we find that the time delay can play an important role in reducing the peak load. Finally, the relationship of our system to previous studies on coupled oscillators are explained in detail.

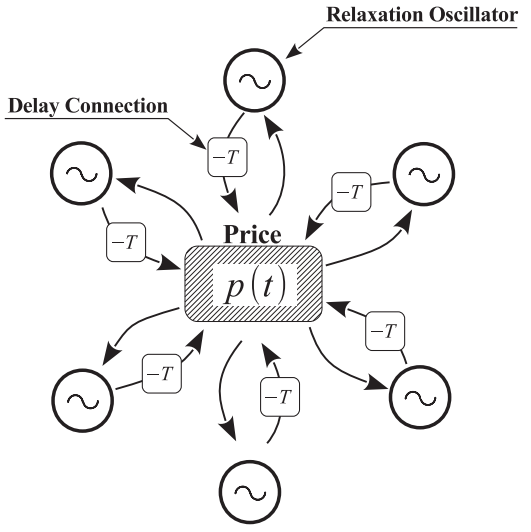

FIG. 2. Globally delay-coupled relaxation oscillators

II. MATHEMATICAL MODEL

We begin by considering the situation, illustrated in Fig. 1, in which N users receive power from a power grid; moreover, each user possesses a storage (e.g., battery or thermal storage) and constantly consumes power V. The energy stored in the storage, $X_i(\tau) \in [0,\bar{X}]$, with the storage capacity $\bar{X} > 0$, of user $i \in \{1,\ldots,N\}$ at time τ can be written as

$$X_i(\tau) = X_i(0) - V\tau + \int_0^\tau U_i(\tau')d\tau', \tag{1}$$

where $X_i(0)$ is the initial stored energy. $U_i(\tau) \in \{0,\bar{U}_i\}$ is the received power, where $\bar{U}_i$ denotes the charging power. The total power flow from the power grid to all of the storages is given by

$$U_{\text{total}}(\tau) = \sum_{i=1}^{N} U_i(\tau). \tag{2}$$

We suppose that every user acts independently for its own profit based on two simple rules. First, each user aims to reduce the repetition of charge and noncharge actions, because an increase in repetition accelerates storage degradation (e.g., for batteries) and increases power loss in converting energy (e.g., for thermal storages). Second, each user begins charging his or her own storage when the power price is less than a price threshold. This paper investigates the dynamical behavior of storage state (1) with these two rules.

Here we propose a power price,

$$P(\tau) = \frac{1}{N} U_{\text{total}}(\tau - \Gamma), \tag{3}$$

proportional to the past (i.e., delayed) total power flow, where $\Gamma \geqslant 0$ is the length of time required for a power supplier to detect the total power flow and to inform the price to the users. Without loss of generality, we can suppose that $V < \bar{U}_1 < \cdots < \bar{U}_N$. The storage has charge and noncharge states. For a charge state [i.e., $U_i(\tau) = \bar{U}_i$], the storage energy $X_i(\tau)$ increases and reaches the full-charge state [i.e., $X_i(\tau) = \bar{X}$]. Then the storage state changes to noncharge [i.e., $U_i(\tau) = 0$], and the storage energy $X_i(\tau)$ decreases and reaches a state threshold $X_c \in (0,\bar{X})$. The storage begins to be charged only if $X_i(\tau) \leqslant X_c$ and $P(\tau) \leqslant P_c$. If its storage is empty [i.e., $X_i(\tau) = 0$], the storage begins to be charged independent of the price $P(\tau)$.

To simplify the analysis of dynamical behavior, we define the transformation of the variables and the parameters by

$$x_i := \frac{X_i}{\bar{X}} \in [0,1],\ u_i := \frac{U_i}{V} \geqslant 0,\ p := \frac{P}{V} \geqslant 0, \tag{4}$$

$$t := \frac{V\tau}{\bar{X}} \geqslant 0,\ T := \frac{V\Gamma}{\bar{X}} \geqslant 0,\ p_c := \frac{P_c}{V} \geqslant 0, \tag{5}$$

$$x_c := \frac{X_c}{\bar{X}} \in (0,1),\ \bar{u}_i := \frac{\bar{U}_i}{V} \geqslant 0, \tag{6}$$

so we obtain a simple normalized model,

$$\frac{dx_i(t)}{dt} = u_i(t) - 1, \tag{7}$$

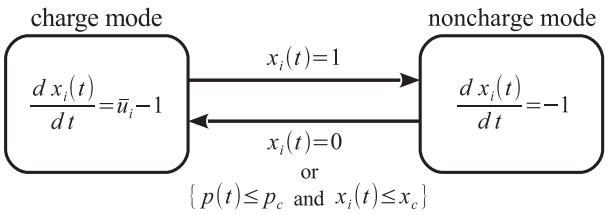

FIG. 3. Dynamics of normalized i-th storage system (7)–(10).

with normalized storage state $x_i(t)$ and normalized time t. The normalized received power is

$$u_i(t)=\begin{cases}\bar{u}_i & \text{if charge mode}\\ 0 & \text{if noncharge mode}\end{cases}, \tag{8}$$

where $\bar{u}_i > 1$ is the normalized charging power. The normalized power price $p(t)$ is

$$p(t)=\frac{1}{N}u_{\text{total}}(t-T),\ u_{\text{total}}(t):=\sum_{i=1}^{N}u_i(t). \tag{9}$$

The charge and noncharge modes of storage i are switched by the following law, as illustrated in Fig. 3:

$$\begin{aligned}&\text{(1) noncharge mode} \Rightarrow \text{charge mode}\\ &\quad\text{if}\quad \{p(t)\leqslant p_c \text{ and } x_i(t)\leqslant x_c\} \text{ or } \{x_i(t)=0\}.\\ &\text{(2) charge mode} \Rightarrow \text{noncharge mode}\\ &\quad\text{if}\quad x_i(t)=1.\end{aligned} \tag{10}$$

Note that the six parameters ($\bar{X}$, V, $\bar{U}_i$, Γ, X_c, P_c) in our system are reduced to only four parameters ($\bar{u}_i$, T, x_c, p_c) in the normalized system. This will simplify our analysis. Figure 4 sketches the time-series data of storage state $x_i(t)$, price $p(t)$, and received power $u_i(t)$. The state of each storage seesaws repeatedly between low-charge level $x_i(t) \in [0,x_c]$ and full-charge level $x_i(t)=1$. In other words, each storage inevitably induces a self-oscillation and behaves as a relaxation oscillator. In addition, the price $p(t)$, which includes past information about all the storages, has an influence on each storage. Therefore, the normalized system (7)–(10) can be considered a globally delay-coupled relaxation oscillator, as illustrated in Fig. 2. This paper investigates the dynamics of oscillators (7)–(10) analytically.

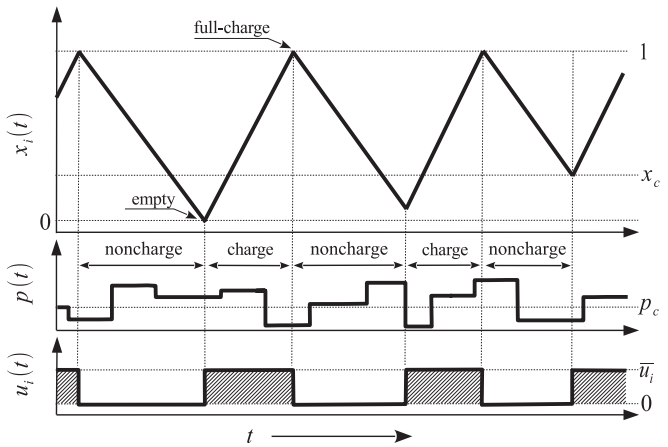

FIG. 4. Sketch of time-series data of storage state $x_i(t)$, price $p(t)$, and charging power $u_i(t)$.

III. DYNAMICAL BEHAVIOR

This section provides preliminaries and proposes an analytical framework. For simplicity, we restrict our attention to the simplest situation $N=2$.

A. Numerical examples

As a beginning, we observe the dynamical behavior of the normalized system (7)–(10) in numerical simulations. The parameters, charging powers and price threshold, are set to

$$\bar{u}_1=2.5000,\ \bar{u}_2=2.6250,\ p_c=0.25\bar{u}_1. \tag{11}$$

Figures 5(a) and 5(b) show the time-series data of storage states $x_{1,2}(t)$ and total power flow $u_{\text{total}}(t)$ with $N=2$ for $(x_c,T)=(0.30,0.05)$ and $(x_c,T)=(0.10,0.40)$, respectively. Without using price, the two storages oscillate independently for $t<5$. Moreover, we see that the peak load occurs when they are simultaneously in the charge mode. They are controlled with price (9) for $t \geqslant 5$. The peak load is suppressed in the steady state as shown in Fig. 5(a), but it still occurs in Fig. 5(b). These differing results indicate that we must choose the appropriate parameters, $\bar{u}_{1,2}$, p_c, x_c, and T, to suppress the peak load. The primary purpose of this paper is to clarify

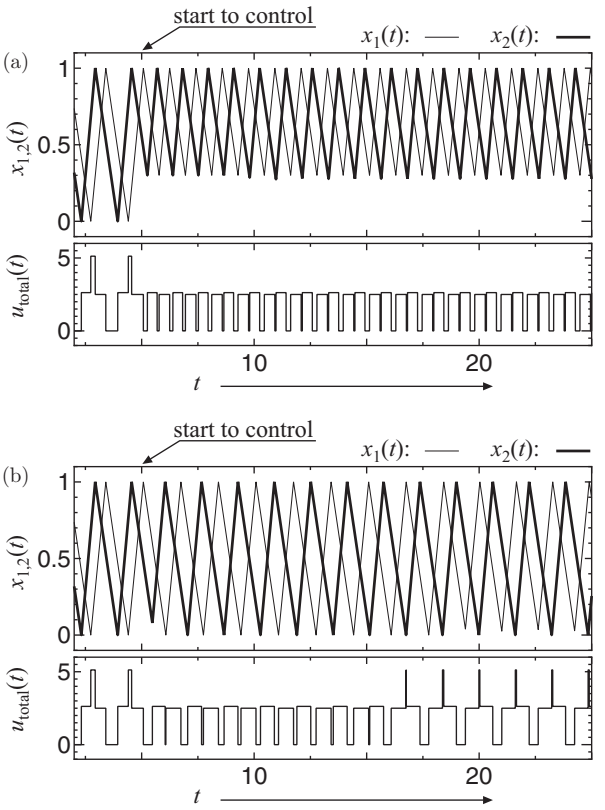

FIG. 5. Time-series data of storage states $x_{1,2}(t)$ and total power flow $u_{\text{total}}(t)$ with $N=2$: (a) $(x_c,T)=(0.30,0.05)$ and (b) $(x_c,T)=(0.10,0.40)$.

the peak-generating mechanism and to design the parameters for suppressing the peak load.

B. Assumptions and definition

Let us assume the following.

Assumption 1. Assume that the charging powers $\bar{u}_{1,2}$ and the price threshold p_c satisfy

$$2 < \bar{u}_1 < \bar{u}_2,\ p_c \in \left(0, \frac{1}{2}\bar{u}_1\right). \tag{12}$$

The first condition in (12) means that the charge periods of storages are less than the noncharge periods. It is necessary that the two storages do not charge simultaneously. The second condition in (12) is also necessary for the two storages to affect each other. To simplify our analysis, we now define the following parameters:

$$\bar{u}_1^* := \frac{1}{\bar{u}_1 - 1} \in (0,1), \quad \bar{u}_2^* := \frac{1}{\bar{u}_2 - 1} \in (0,1). \tag{13}$$

Assumption 1 guarantees that $0 < \bar{u}_2^* < \bar{u}_1^* < 1$.

The peak load is defined as follows.

Definition 1. If there exists time t^* such that the total power flow $u_{\text{total}}(t)$ defined by Eq. (9) with $N = 2$ is less than or equal to $\bar{u}_2$ for any time $t \geqslant t^*$, that is,

$$u_{\text{total}}(t) \leqslant \bar{u}_2,\ \forall t \geqslant t^*,$$

then the peak load (i.e., simultaneous charging) does not occur in a steady state.

It is easy to see that a sufficiently short delay (i.e., $T \ll 1$) might not induce the peak load. For long delays, however, we cannot intuitively see whether the peak load occurs. Now we attempt to reveal its dynamics, because this would be important information for designing our system.

Moreover, we introduce the following assumption.

Assumption 2. Delay time T satisfies

$$T \in \left(0, \frac{1}{2}(1 - x_c)\right). \tag{14}$$

This assumption will simplify our analysis of the dynamics, as we see later. The upper limit of time-delay range (14) is one-half of the time required for a fully charged storage to reach the threshold x_c. Thus, this assumption is not a strict condition.

C. Dynamics on phase plane

This subsection investigates the dynamics in a pair of storages on a phase plane. Figure 6 illustrates the trajectory of the storages on the phase plane $x_1(t) - x_2(t)$. The dynamics can be understood in detail with reference to Fig. 6.

A: Storage 1 is in the full-charge state, and storage 2 is in noncharge mode.

A $\rightarrow$ B: Both storages are in noncharge mode.

B: Storage 2 reaches the state threshold, $x_2(t) = x_c$, and then begins to charge in response to the low price $p(t) = 0$. Note that this price depends on the past states of these storages, that is, the point b at which both storages are in noncharge mode.

B $\rightarrow$ C: Storage 1 is in noncharge mode, and storage 2 is in charge mode.

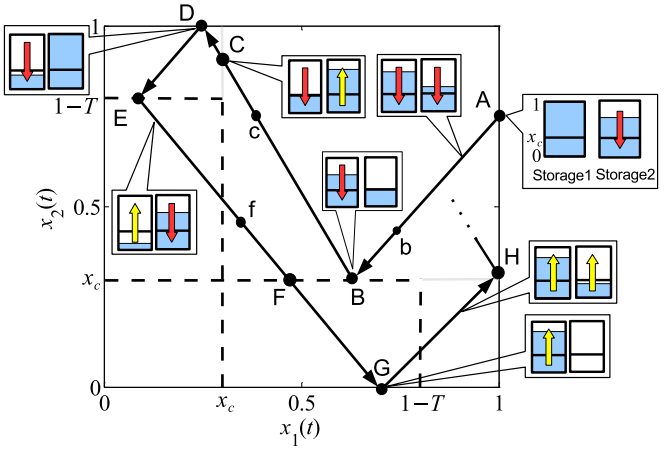

FIG. 6. Schematic illustration of trajectory of two storages on phase plane.

C: Storage 1 reaches the state threshold, $x_1(t) = x_c$, but cannot begin charging because of the high price, $p(t) = \bar{u}_2/2 > p_c$. This is because the past state of storage 2 at point c is in charge mode.

C $\rightarrow$ D: Storage 1 is in no-charge mode and storage 2 is in charge mode.

D: Storage 2 reaches the full-charge state, $x_2(t) = 1$, and then changes to noncharge mode.

D $\rightarrow$ E: Both storages are in noncharge mode.

E: Storage 1 begins charging, because the price turns changes to low, $p(t) = 0$. The reason is that the past state of storage 2 at point D turns to noncharge mode.

E $\rightarrow$ F: Storage 1 is in charge mode, and storage 2 is in noncharge mode.

F: Storage 2 reaches the state threshold, $x_2(t) = x_c$, but cannot begin charging because of the high price, $p(t) = \bar{u}_1/2 > p_c$. This is because the past state of storage 1 at point f is in charge mode.

F $\rightarrow$ G: Storage 1 is in charge mode, and storage 2 is in noncharge mode.

G: Storage 2 is empty, $x_2(t) = 0$, and then begins charging independent of the price.

G $\rightarrow$ H: Both storages are in charge mode, resulting in peak load.

As aforementioned, the behavior of these storages can be expressed as a trajectory on the phase plane.

IV. DESIGN OF SYSTEM PARAMETERS

This section presents a systematic procedure for designing the system parameters, x_c and T, under Assumptions 1 and 2 such that the peak load described in Definition 1 does not occur. It is easy to understand that both of the following conditions are satisfied if the peak load does not occur.

Condition (a): There does not exist a time interval in which both storages are in charge mode simultaneously (i.e., there is no trajectory that has a positive slope with an increase such as G $\rightarrow$ H in Fig. 6).

Condition (b): The dynamics settles in a steady state (i.e., a stable limit cycle appears on the phase plane).

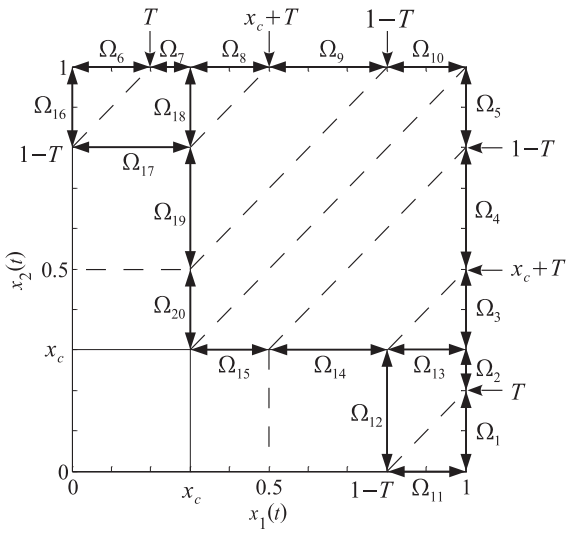

FIG. 7. Definition of regions Ω_i ($i = 1, \ldots, 20$).

First, we deal with Condition (a). Let us define a Poincare section as follows:

$$\Sigma := \{(x_1, x_2) \in \boldsymbol{R}^2 : x_1 = 1, x_2 \in [0,1], \dot{x}_2 < 0\}. \quad (15)$$

As the trajectories with *positive* slopes (i.e., $\dot{x}_2 > 0$) induce the peak load, in this section, the trajectories are restricted to those with *negative* slopes (i.e., $\dot{x}_2 < 0$) at $x_1 = 1$ from the segment $x_2 \in [0,1]$ at $x_1 = 1$. Let us define a return map, $F : \Sigma \to \Sigma$, by

$$x_2[n+1] = F(x_2[n]), \quad (16)$$

where the state of the map is defined by $x_2[n] := x_2(t_n)$ on Σ at the n-th time, t_n. Now we specify this map. Let us define regions Ω_i ($i = 1, \ldots, 20$) under Assumption 2 [2] as illustrated in Fig. 7. We find that there are nine potential cases for which trajectories from Σ to Σ do not include any positive slopes:

$$\text{Case 1}: \ \Omega_1 \to \Omega_{11} \to \Omega_6 \to \Omega_{16} \to \Omega^*, \quad (17)$$

$$\text{Case 2}: \ \Omega_1 \to \Omega_{11} \to \Omega_7 \cup \Omega_8 \to \Omega_{17} \to \Omega^*, \quad (18)$$

$$\text{Case 3}: \ \Omega_1 \to \Omega_{11} \to \Omega_9 \cup \Omega_{10} \to \Omega_{19} \cup \Omega_{20} \to \Omega^*, \quad (19)$$

$$\text{Case 4}: \ \Omega_2 \cup \Omega_3 \to \Omega_{12} \to \Omega_6 \to \Omega_{16} \to \Omega^*, \quad (20)$$

$$\text{Case 5}: \ \Omega_2 \cup \Omega_3 \to \Omega_{12} \to \Omega_7 \cup \Omega_8 \to \Omega_{17} \to \Omega^*, \quad (21)$$

$$\text{Case 6}: \ \Omega_2 \cup \Omega_3 \to \Omega_{12} \to \Omega_9 \to \Omega_{19} \to \Omega^*, \quad (22)$$

$$\text{Case 7}: \ \Omega_3 \cup \Omega_4 \to \Omega_{13} \cup \Omega_{14} \to \Omega_6 \to \Omega_{16} \to \Omega^*, \quad (23)$$

$$\text{Case 8}: \ \Omega_3 \cup \Omega_4 \to \Omega_{13} \cup \Omega_{14} \to \Omega_7 \cup \Omega_8 \to \Omega_{17} \to \Omega^*, \quad (24)$$

$$\text{Case 9}: \ \Omega_3 \cup \Omega_4 \cup \Omega_5 \to \Omega_{13} \cup \Omega_{14} \cup \Omega_{15} \to \Omega_8 \cup \Omega_9 \cup \Omega_{10} \to \Omega_{18} \cup \Omega_{19} \cup \Omega_{20} \to \Omega^*, \quad (25)$$

where $\Omega^* := \Omega_1 \cup \Omega_2 \cup \Omega_3 \cup \Omega_4 \cup \Omega_5$. Each case provides a path of trajectories on the phase plane. For instance, Case 1 [see Eq. (17)] indicates that trajectories visit the regions, Ω_1, Ω_{11}, Ω_6, Ω_{16}, and Ω^*, in sequence. The return map F can be described by

$$F(x) = \begin{cases} f_1(x) & \text{for} \quad \text{Case 1} \\ f_2(x) & \text{for} \quad \text{Case 2} \\ \vdots & \\ f_9(x) & \text{for} \quad \text{Case 9} \end{cases},$$

where map f_j for case j is defined by

$$f_1(x) = x - \bar{u}_1^* + \bar{u}_2^*, \quad (26)$$

$$f_2(x) = -\bar{u}_1^* x - (1 + \bar{u}_1^*)T + 1 - \bar{u}_1^* \bar{u}_2^*, \quad (27)$$

$$f_3(x) = x + (1 + \bar{u}_1^*)x_c - \bar{u}_1^* + \bar{u}_2^*, \quad (28)$$

$$f_4(x) = -\bar{u}_2^* x + (1 + \bar{u}_2^*)T - \bar{u}_1^* + \bar{u}_2^*, \quad (29)$$

$$f_5(x) = \bar{u}_1^* \bar{u}_2^* x - (1 + 2\bar{u}_1^* + \bar{u}_1^* \bar{u}_2^*)T + 1 - \bar{u}_1^* \bar{u}_2^*, \quad (30)$$

$$f_6(x) = -\bar{u}_2^* x + (1 + \bar{u}_2^*)T + (1 + \bar{u}_1^*)x_c - \bar{u}_1^* + \bar{u}_2^*, \quad (31)$$

$$f_7(x) = x - (1 + \bar{u}_2^*)x_c - \bar{u}_1^* + \bar{u}_2^*, \quad (32)$$

$$f_8(x) = -\bar{u}_1^* x - (1 + \bar{u}_1^*)T + \bar{u}_1^*(1 + \bar{u}_2^*)x_c + 1 - \bar{u}_1^* \bar{u}_2^*, \quad (33)$$

$$f_9(x) = x + (\bar{u}_1^* - \bar{u}_2^*)x_c - \bar{u}_1^* + \bar{u}_2^*. \quad (34)$$

The case number j depends on the system parameters (i.e., x_c, T, $\bar{u}_{1,2}$) and the state $x_2[n]$.

Second, we consider Condition (b). If the map f_j has the stable fixed point x_j^* satisfying

$$x_j^* = f_j(x_j^*), \quad (35)$$

then there exists a stable limit cycle on the phase plane [i.e., Condition (b) holds]. Now we investigate the existence of the fixed point for all cases ($j = 1, \ldots, 9$).

The analytical results for Cases 1, 3, 4, 7, 8, and 9 are provided below.

Lemma 1. There does not exist a fixed point for Cases 1, 3, 4, 7, 8, and 9 under Assumption 1.

Proof. See Appendix A 1.

The existence of stable fixed points for Cases 2, 5, and 6 is explained by the following lemmas.

[2] The upper limit of T in Assumption 2, which is equivalent to $x_c + T < 1 - T$, indicates that the regions $\Omega_{4,9,14,19}$ exist as shown in Fig. 7. Throughout this paper, the existence of limit cycles and their stability are analyzed on the basis of regions Ω_i ($i = 1, \ldots, 20$) defined by Fig. 7.

Lemma 2. There exists a stable fixed point x_2^* for Case 2 if the parameters x_c and T satisfy

$$x_c \in \left(\frac{\bar{u}_1^* - \bar{u}_2^*}{1+\bar{u}_1^*}, 1\right), \tag{36a}$$

$$T \in \left(\frac{1-\bar{u}_1^*\bar{u}_2^*}{2(1+\bar{u}_1^*)}, \frac{1-\bar{u}_1^*\bar{u}_2^*}{1+\bar{u}_1^*}\right), \tag{36b}$$

under Assumptions 1 and 2.

Proof. See Appendix A 2.

Lemma 3. There exists a stable fixed point x_5^* for Case 5 if the parameter T satisfies

$$T \in \left(\frac{(1-\bar{u}_1^*\bar{u}_2^*)(1-x_c)}{2(1+\bar{u}_2^*)}, \frac{1-\bar{u}_1^*\bar{u}_2^*}{2(1+\bar{u}_1^*)}\right), \tag{37}$$

under Assumptions 1 and 2.

Proof. See Appendix A 3.

Lemma 4. There exists a stable fixed point x_6^* for Case 6 if the parameters x_c and T satisfy

$$x_c \in \left(\frac{\bar{u}_1^* - \bar{u}_2^*}{1+\bar{u}_1^*}, 1\right), \tag{38a}$$

$$T \in \left(0, \frac{(1-\bar{u}_1^*\bar{u}_2^*)(1-x_c)}{2(1+\bar{u}_2^*)}\right), \tag{38b}$$

under Assumptions 1 and 2.

Proof. See Appendix A 4.

These lemmas yield the following main result.

Theorem 1. There exists a stable fixed point if the parameters x_c and T satisfy

$$x_c \in (x_c^*, 1),\ x_c^* := \frac{\bar{u}_1^* - \bar{u}_2^*}{1+\bar{u}_1^*} = \frac{\bar{u}_2/\bar{u}_1 - 1}{\bar{u}_2 - 1}, \tag{39}$$

$$T \in (0, T^*),\ T^* := \frac{1-\bar{u}_1^*\bar{u}_2^*}{1+\bar{u}_1^*} = 1 - \frac{1}{\bar{u}_1 - \bar{u}_1/\bar{u}_2}, \tag{40}$$

under Assumptions 1 and 2.

Proof. This is obvious from Lemmas 2, 3, and 4.

This theorem provides a procedure for designing the system parameters x_c and T.

(Step 1) The charging powers $\bar{u}_{1,2}$ and the price threshold p_c are given.

(Step 2) If they do not satisfy Assumption 1, then we abandon our design.

(Step 3) Design the state threshold x_c such that condition (39) holds.

(Step 4) Design the delay time T such that both Assumption 2 and condition (40) hold.

The analytical results aforementioned are confirmed numerically in the next section.

V. NUMERICAL RESULTS AND DISCUSSION

This section verifies the analytical results for $N = 2$ numerically. Moreover, the dynamical behavior for $N > 2$ is investigated through numerical simulations. Finally, some potential contributions of our proposal and previous work related to our system in the field of nonlinear science are summarized.

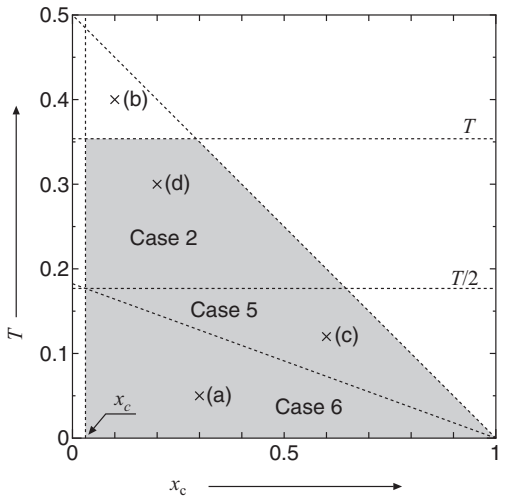

FIG. 8. Regions for Lemmas 2 (Case 2), 3 (Case 5), 4 (Case 6), and Theorem 1 (gray area) in parameter space $x_c - T$ ($\bar{u}_1 = 2.500$, $\bar{u}_2 = 2.625$): (a) $(x_c, T) = (0.30, 0.05)$, (b) $(x_c, T) = (0.10, 0.40)$, (c) $(x_c, T) = (0.60, 0.12)$, and (d) $(x_c, T) = (0.20, 0.30)$.

A. Case of $N = 2$

For $N = 2$, we can design the system parameters x_c and T in accordance with Theorem 1. For (Step 1), the charging power and the price threshold are given as in Eq. (11) in Sec. III A. For (Step 2), we confirm that they satisfy Assumption 1 and then proceed to the next step. For (Step 3), the state threshold x_c is chosen from condition (39),

$$x_c \in (x_c^*, 1),\ x_c^* = 0.0308. \tag{41}$$

For (Step 4), from Assumption 2 and condition (40), we see that the delay time T is taken from

$$T \in \left(0, \min\left\{T^*, \frac{1}{2}(1-x_c)\right\}\right), \quad T^* = 0.3538. \tag{42}$$

Figure 8 illustrates a region (gray area) derived from Theorem 1 on parameter space $x_c - T$. Notice that if x_c and T are chosen from the gray region, then the peak load never occurs in a steady state. The time-series data for the parameter sets (a) $(x_c, T) = (0.30, 0.05)$ and (b) $(x_c, T) = (0.10, 0.40)$ in Fig. 8, as shown in Figs. 5(a) and 5(b), agree with the analytical result of Theorem 1.

This stability region can be divided into the three subregions corresponding to the three cases of limit cycles, Lemma 2 (Case 2), Lemma 3 (Case 5), and Lemma 4 (Case 6). Let us numerically review the dynamics in each subregion. Figure 9(a) shows the trajectory in a steady state on the phase plane for the parameter set (a) $(x_c, T) = (0.30, 0.05)$ in Fig. 8 [see also Fig. 5(a)]. It can be seen that the trajectory has the following characteristics: It does not have a positive slope with an increase [Condition (a)], it forms a stable limit cycle [Condition (b)], and it visits the regions of Case 6 defined by Eq. (22) (Lemma 4). Moreover, the trajectory for the parameter set (b) $(x_c, T) = (0.10, 0.40)$ in Fig. 8 [also see Fig. 5(b)] is shown in Fig. 9(b): It has a positive slope with an increase [i.e., Condition (a) does not hold], and it forms a stable limit cycle [Condition (b)]. The trajectories for the parameter sets (c) and (d) are shown in Figs. 9(c) and 9(d), respectively: They

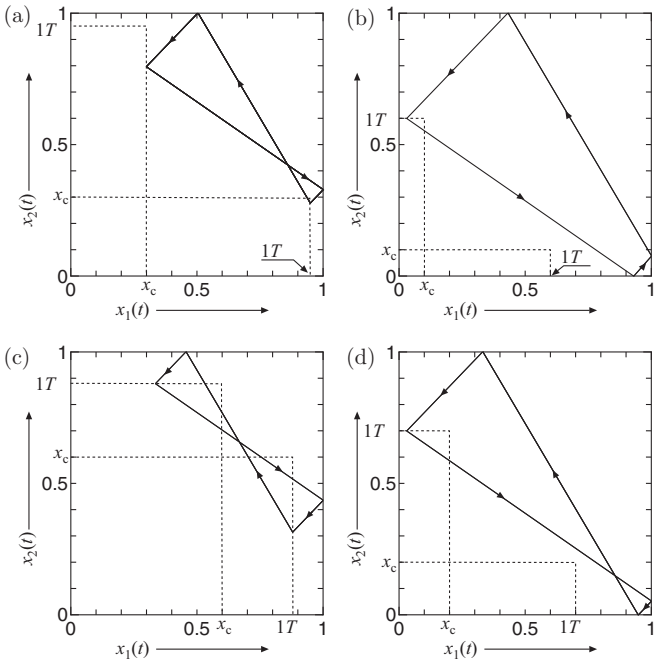

FIG. 9. Trajectories in steady state on the phase plane ($\bar{u}_1 = 2.500$, $\bar{u}_2 = 2.625$): (a) $(x_c, T) = (0.30, 0.05)$, (b) $(x_c, T) = (0.10, 0.40)$, (c) $(x_c, T) = (0.60, 0.12)$, (d) $(x_c, T) = (0.20, 0.30)$.

do not have a positive slope with an increase [Condition (a)], they form stable limit cycles [Condition (b)], and they visit the regions of Cases 5 and 2 defined by Eqs. (21) and (18) (Lemmas 3 and 2), respectively. These numerical results agree with the analytical results.

Let us numerically confirm that the peak load in the steady state never occurs in the stability region. We now define a peak load in the steady state,

$$\hat{u}_{\text{total}} := \max_{t \in [t_{\min}, t_{\max}]} u_{\text{total}}(t), \tag{43}$$

where the upper and lower limits, $t_{\min}$ and $t_{\max}$, of the time interval are set to $0 \ll t_{\min} < t_{\max}$ to ignore the transient behavior. The peak load $\hat{u}_{\text{total}}$ might depend on the initial states, $x_i(0)$ and charge and noncharge modes; thus, we will estimate the averaged peak load, $\langle \hat{u}_{\text{total}} \rangle$. The initial states, $x_i(0) \in [0,1]$ and charge and noncharge modes are randomly chosen, and each storage behaves independently without using the price for $t < 100$. These storages begin to be controlled using price at $t = 100$. The limits of the time interval are set to $t_{\min} = 1500$ and $t_{\max} = 2000$. The averaged peak load $\langle \hat{u}_{\text{total}} \rangle$ is estimated by repeating the above procedure 10 times. The peak load $\langle \hat{u}_{\text{total}} \rangle$ is plotted as a function of x_c and T in Fig. 10(a). The dark (light) region indicates low (high) peak load. This result leads to the conclusion that the analytical result of Theorem 1 agrees well with the numerical result.

B. Case of $N > 2$

We have shown that our analytical results are valid for a pair of storages ($N = 2$). However, for $N > 2$, we cannot analytically guarantee whether they are valid. Let us consider the dynamics of $N = 10$ storages with the price threshold $p_c = 0.49\bar{u}_1$ through numerical simulations. The averaged peak load $\langle \hat{u}_{\text{total}} \rangle$ is estimated by repeating the following procedure 10 times: $x_i(0) \in [0,1]$ ($i = 1, \ldots, 10$), charge and noncharge modes, and the charging powers $\bar{u}_i \in [2.5000, 2.8000]$ ($i = 1, \ldots, 10$) are randomly chosen.

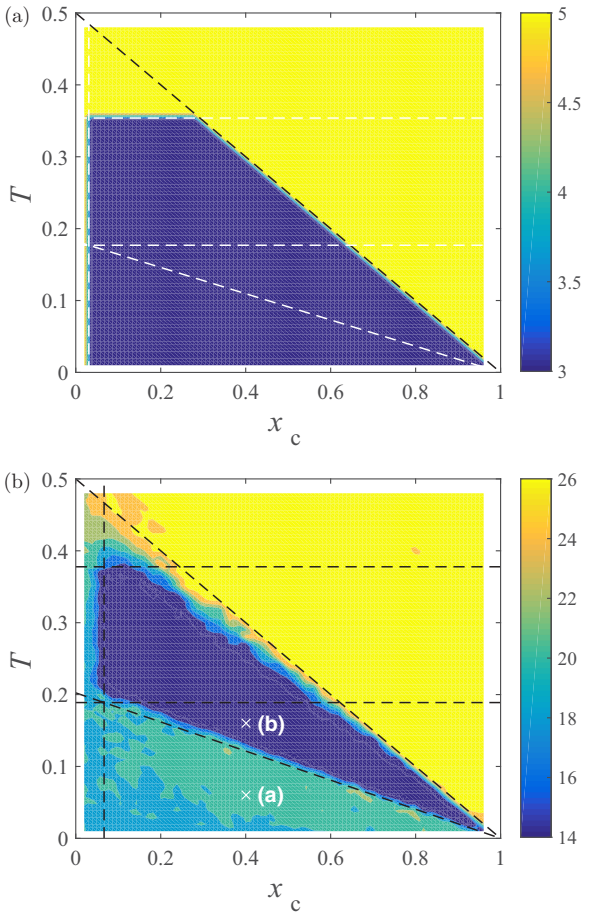

FIG. 10. Plots of averaged peak load $\langle \hat{u}_{\text{total}} \rangle$ on parameter space x_c vs T for (a) $N = 2$ with $\bar{u}_{1,2} = 2.5000, 2.6250$ and (b) $N = 10$ with $\bar{u}_{1,\ldots,10} \in [2.5000, 2.8000]$.

The peak load $\langle \hat{u}_{\text{total}} \rangle$ is plotted as a function of x_c and T in Fig. 10(b). The analytical boundary lines with $N = 2$, $\bar{u}_1 = 2.5000$, and $\bar{u}_2 = 2.800$, calculated by Lemmas 2 (Case 2), 3 (Case 5), and 4 (Case 6), are also described in this figure solely to provide information. The dark (light) region indicates that the peak load is low (high). We roughly see that the peak load $\langle \hat{u}_{\text{total}} \rangle$ is low in the region of Cases 5 and 2 as compared with the region of Case 6. Figures 11(a) and 11(b) show the time-series data of $x_{1,\ldots,10}(t)$ and $u_{\text{total}}(t)$ at (a) $(x_c, T) = (0.40, 0.06)$ and (b) $(x_c, T) = (0.40, 0.16)$, respectively, shown in Fig. 10(b). For a short delay $T = 0.06$, as shown in Fig. 11(a), the storages are not synchronized; thus, the total power flow occasionally shows peaks. Conversely, for a long delay $T = 0.16$, all the storages behave as two-phase oscillations with antiphase synchronization as shown in Fig. 11(b); moreover, each phase includes five storages, and the peak load does not occur. We notice that the two-phase oscillators behave as a pair of storages in Case 5 [cf., Fig. 9(c)].

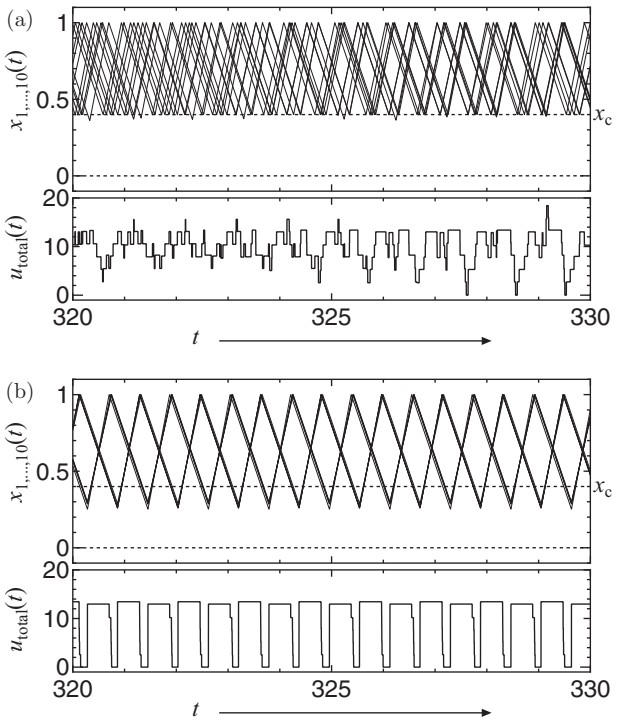

FIG. 11. Time-series data of the storage states $x_{1,\ldots,10}(t)$ and the total power flow $u_{\text{total}}(t)$ with $N = 10$ and $x_c = 0.40$: (a) $T = 0.06$ and (b) $T = 0.16$.

In general, the analysis of dynamical systems including delays [35] is difficult because of their infinite-dimensional dynamics [36–38]; furthermore, it is well accepted that time delay in engineering systems is regarded as harmful to system stability. Note that $\langle \hat{u}_{\text{total}} \rangle$ for parameter set $(x_c, T) = (0.40, 0.16)$ (i.e., long delay) is lower than that at $(x_c, T) = (0.40, 0.06)$ (i.e., short delay). This fact implies that the time delay T can induce synchronization and reduce the peak load.

C. Discussion

This section will summarize some potential contributions of our proposal to power systems research. Moreover, we will mention the relationship of our power system to previous studies in nonlinear science.

The core idea of this paper involves the application of knowledge of nonlinear science to a problem in the power systems research. Although our system might be regarded as an interdisciplinary study, it is still at the most fundamental level and has substantial room for improvement. In particular, antiphase synchronization, one of the nonlinear phenomena that occur in coupled oscillators, can be useful in reducing the peak of total power flow. This result provides the potential of using substantial nonlinear phenomena to solve various problems in power systems research. As most nonlinear phenomena are induced by simple rules (e.g., coupled nonlinear oscillators, coupled nonlinear maps, and reaction-diffusion systems), the main advantage of using nonlinear phenomena might be simplification of the control law and system structure even for large power systems.

Note that our study deals with an interesting nonlinear system, relaxation oscillators coupled by a time-delay global-repulsive connection, as sketched in Fig. 2. From the viewpoint of nonlinear dynamics, we now consider the relation between our system and previous studies.

Relaxation oscillators, which have slow and fast time scales, have been well known in nonlinear science [32,33]. The storages in our system also have two such time scales, such as states in charge and noncharge modes (i.e., slow scale) and jumps between these modes (i.e., fast scale). Hence, these storages can be regarded as a type of relaxation oscillators.

Time-delay connections have attracted attention in the field of nonlinear dynamics [37], because they induce several interesting phenomena, such as coexistence of several synchronizations [39], enhancement of synchronization [40–42], time-delay-induced phase transition [43], and induction of stabilization [44–46]. We observe that the time delay in connection would be the key to the suppression of the peak load in our system with $N = 10$.

Connection topologies in networks are classified into local, global, and intermediate connections [1,3]. It is widely accepted that the dynamics of networks strongly depends on connection type. The connection in our system is considered not only as a global connection but also a delay connection [47,48], because the price sent to each user includes the delayed sum of the received power flows of all users.

The interactions in connection are divided into three cases, attractive, repulsive, and mixed: The attractive interaction induces in-phase synchronization, as it tends to pull the oscillator phases together; the repulsive interaction induces the antiphase synchronization due to push action [49,50]; and their mixed interaction causes interesting phenomena [51]. The price in our system, which is proportional to the past total power-flow, acts to push the phases of charge mode apart. Hence, the interaction between the storages is considered as a repulsive connection with delay [34].

As mentioned, each of the key subjects in our systems have been investigated already in detail; thus, a substantial amount of knowledge has been accumulated on each. The time-delay-induced suppression of peak load observed in our system, as shown in Fig. 11(b), does not contradict the results of the previous study, the enhancement of synchronization by a repulsive delay connection [34]; however, other accumulated deep knowledge on each subject has not been sufficiently utilized in analyzing and designing our system. It is expected that such knowledge will allow us to improve our analysis and design, which will lead to the improvement of system performance.

VI. CONCLUSION

This paper investigated the dynamical behavior of a pair of storages from the viewpoint of nonlinear dynamics. A systematic procedure for designing the system parameters was provided. The analytical results suggest that the peak load can be reduced even if the real-time pricing systems involve delay time.

APPENDIX A: PROOFS OF LEMMAS

This Appendix provides proofs of lemmas.

1. Proof of Lemma 1

First, we consider cases 1, 3, 7, and 9. As the maps $f_{1,3,7,9}$ described by Eqs. (26), (28), (32), and (34) have gradient 1 and some bias, there does not exist a stable isolated fixed point (35). Second, we consider Case 4. The map f_4 does not have a fixed point x_4^* in the region $\Omega_2 \cup \Omega_3 = [T, x_c + T]$ under $\bar{u}_2^* < \bar{u}_1^*$ ($\Leftrightarrow \bar{u}_1 < \bar{u}_2$) in Assumption 1. Third, we consider Case 8. The trajectory from the fixed point x_8^* never visit $\Omega_7 \cup \Omega_8$ under $\bar{u}_2^* < \bar{u}_1^*$ ($\Leftrightarrow \bar{u}_1 < \bar{u}_2$) in Assumption 1 and under definition (6). This implies that a fixed point x_8^* for Case 8 does not exist. In conclusion, fixed points $x_{1,3,4,7,8,9}^*$ do not exist under Assumption 1.

2. Proof of Lemma 2

We show the existence of a limit cycle that visits the regions described by Eq. (18) and its stability for Case 2. It is easily confirmed by simple manipulations that if T satisfies condition (36b), then a fixed point x_2^* satisfying $x_2^* = f_2(x_2^*)$ exists within the region Ω_1. The trajectory starting from x_2^* in section Σ inevitably visits the region Ω_{11}. We easily see that if x_c satisfies condition (36a) under Assumption 2 and $0 < \bar{u}_2^* < \bar{u}_1^* < 1$ in Assumption 1 holds, then the trajectory visits the region $\Omega_7 \cup \Omega_8$. Moreover, we easily confirm that the trajectory visits the region Ω_{17} and returns to x_2^*. These facts guarantee that under Assumptions 1 and 2, if the two conditions (36a) and (36b) hold, then the limit cycle starting from x_2^* and returning to x_2^* exists. In addition, it is guaranteed that the limit cycle is stable, as the map f_2 defined by Eq. (27) has the gradient $-\bar{u}_1^* \in (-1,0)$.

3. Proof of Lemma 3

As in the proof of Appendix A 2, for Case 5, the existence of the limit cycle visiting the regions described by Eq. (21) and its stability will be proved. We see that if T satisfies condition (37) under Assumptions 1 and 2, then the fixed point x_5^* satisfying $x_5^* = f_5(x_5^*)$ exists within the region $\Omega_2 \cup \Omega_3$. The trajectory starting from x_5^* inevitably visits the region Ω_{12}. In addition, we can see that if T satisfies condition (37), then the trajectory visits the region $\Omega_7 \cup \Omega_8$. It is clear that the trajectory visits the region Ω_{17} and return to x_5^*. As a result, we notice that under Assumptions 1 and 2, if condition (37) holds, the limit cycle starting from x_5^* and returning to x_5^* exists. In addition, we can guarantee that the limit cycle is stable, as the map f_5 defined by Eq. (30) has the gradient $\bar{u}_1^* \bar{u}_2^* \in (0,1)$.

4. Proof of Lemma 4

The proof follows closely that of Appendix A 2. The existence of a limit cycle visiting the regions described by Eq. (22) and its stability for Case 6 will be provided below. If x_c satisfies condition (38a) under Assumption 2 and $0 < \bar{u}_2^* < \bar{u}_1^* < 1$ in Assumption 1, then the fixed point x_6^* of map f_6 exists within the region $\Omega_2 \cup \Omega_3$. The trajectory starting from x_6^* inevitably visits the region Ω_{12}. Moreover, we see that if the conditions (38a) and (38b) are satisfied, the trajectory visits the region Ω_9. Then the trajectory visits the region Ω_{19} and returns to x_6^*. From these arguments, we can guarantee that if conditions (38a) and (38b) hold under Assumptions 1 and 2, then the limit cycle starting from x_6^* and returning to x_6^* exists. Furthermore, we know that the limit cycle is stable, because the gradient of map f_6 is $-\bar{u}_2^* \in (-1,0)$.

[1] A. Pikovsky, M. Rosenblum, and J. Kurths, *Synchronization* (Cambridge University Press, Cambridge, 2001).

[2] S. H. Strogatz, *Sync: The Emerging Science of Spontaneous Order* (Hyperion, New York, 2003).

[3] G. Osipov, J. Kurths, and C. Zhou, *Synchronization in Oscillatory Networks* (Springer, Berlin, 2007).

[4] A. Arenas, A. Diaz-Guilera, J. Kurths, Y. Moreno, and C. Zhou, Phys. Rep. **469**, 93 (2008).

[5] F. Dorfler and F. Bullo, Automatica **50**, 1539 (2014).

[6] L. M. Pecora and T. L. Carroll, Phys. Rev. Lett. **64**, 821 (1990).

[7] A. Argyris, D. Syvridis, L. Larger, V. Annovazzi-Lodi, P. Colet, I. Fischer, J. Garci'a-Ojalvo, C. R. Mirasso, L. Pesquera, and K. A. Shore, Nature **438**, 343 (2005).

[8] C. Zhou and K. Low, IEEE/ASME Trans. Mechatron. **17**, 25 (2012).

[9] X. Wang, A. Saberi, A. A. Stoorvogel, H. F. Grip, and T. Yang, Automatica **49**, 2461 (2013).

[10] N. F. Rulkov, L. Tsimring, M. L. Larsen, and M. Gabbay, Phys. Rev. E **74**, 056205 (2006).

[11] Y.-T. Lo and J.-F. Kiang, IEEE Trans. Microwave Theor. Tech. **63**, 1353 (2015).

[12] P. Longhini, A. Palacios, V. In, J. D. Neff, A. Kho, and A. Bulsara, Phys. Rev. E **76**, 026201 (2007).

[13] V. In, P. Longhini, A. Kho, N. Liu, S. Naik, A. Palacios, and J. D. Neff, Physica D **240**, 701 (2011).

[14] T. Saito, S. Tasaki, and H. Torikai, IEEE Trans. Circuits Syst. I **52**, 1666 (2005).

[15] T. Saito, Y. Ishikawa, and Y. Ishige, in *Applications of Nonlinear Dynamics*, edited by V. In, P. Longhini, and A. Palacios (Springer, Berlin, 2009), pp. 133–144.

[16] Y. Susuki and I. Mezic, IEEE Trans. Power Syst. **26**, 1894 (2011).

[17] A. Motter, S. Myers, M. Anghel, and T. Nishikawa, Nat. Phys. **9**, 191 (2013).

[18] P. Menck, J. Heitzig, J. Kurths, and H. Schellnhuber, Nat. Commun. **5**, 3969 (2014).

[19] K. Konishi, Y. Sugitani, and N. Hara, Phys. Rev. E **91**, 012911 (2015).

[20] A. Ipakchi and F. Albuyeh, IEEE Power Energ. Mag. **7**, 52 (2009).

[21] B. Roberts and C. Sandberg, Proc. IEEE **99**, 1139 (2011).

[22] W.-Y. Chiu, H. Sun, and H. Poor, *Proceedings of 2012 IEEE International Conference on Smart Grid Communications* (IEEE, Washington DC, 2012), pp. 73–78.
[23] H. Kumar Nunna and S. Doolla, IEEE Trans. Power Deliv. **28**, 939 (2013).
[24] A. Barbato and A. Capone, Energies **7**, 5787 (2014).
[25] C. Adika and L. Wang, Int. J. Electrical Power Energ. Syst. **57**, 232 (2014).
[26] V. Gungor, D. Sahin, T. Kocak, S. Ergut, C. Buccella, C. Cecati, and G. Hancke, IEEE Trans. Indust. Inform. **9**, 28 (2013).
[27] M. Albadi and E. El-Saadany, Electric Power Syst. Res. **78**, 1989 (2008).
[28] K. Takeno, M. Ichimura, K. Takano, and J. Yamaki, J. Power Sources **142**, 298 (2005).
[29] J. Nutaro and V. Protopopescu, IEEE Trans. Power Syst. **24**, 1337 (2009).
[30] Y. Okajima, T. Murao, K. Hirata, and K. Uchida, *Proceedings of IEEE Conference on Decision and Control* (IEEE, Washington DC, 2013), pp. 2384–2390.
[31] C.-K. Zhang, Y. He, L. Jiang, M. Wu, and Q. Wu, J. Franklin Inst. **351**, 4457 (2014).
[32] J. Guckenheimer and P. Holmes, *Nonlinear Oscillations, Dynamical Systems, and Bifurcations of Vector Fields* (Springer, Berlin, 1983).
[33] J. Thompson and H. Stewart, *Nonlinear Dynamics and Chaos* (Wiley, New York, 2001).
[34] Q. Wang, G. Chen, and M. Perc, PLoS One **6**, e15851 (2011).
[35] T. Vyhlídal, J. Lafay, and R. Sipahi, *Delay Systems: From Theory to Numerics and Applications* (Springer, Berlin, 2013).
[36] J. Hale and S. Lunel, *Introduction to Functional Differential Equations* (Springer, Berlin, 1993).
[37] V. Flunkert, I. Fischer, and E. Schöll, Philos. Trans. R. Soc. A **371**, 20120465 (2013).
[38] L. B. Le, K. Konishi, and N. Hara, Phys. Rev. E **87**, 042908 (2013).
[39] H. G. Schuster and P. Wagner, Prog. Theor. Phys. **81**, 939 (1989).
[40] M. Dhamala, V. K. Jirsa, and M. Ding, Phys. Rev. Lett. **92**, 074104 (2004).
[41] Thomas Kauê Dal'Maso Peron, and F. A. Rodrigues, Phys. Rev. E **86**, 016102 (2012).
[42] M. Shrii, D. Senthilkumar, and J. Kurths, Europhys. Lett. **98**, 10003 (2012).
[43] B. Adhikari, A. Prasad, and M. Dhamala, Chaos **21**, 023116 (2011).
[44] D. V. Ramana Reddy, A. Sen, and G. L. Johnston, Phys. Rev. Lett. **80**, 5109 (1998).
[45] W. Zou, D. V. Senthilkumar, Y. Tang, and J. Kurths, Phys. Rev. E **86**, 036210 (2012).
[46] Y. Sugitani, K. Konishi, L. B. Le, and N. Hara, Chaos **24**, 043105 (2014).
[47] M. K. Stephen Yeung and S. H. Strogatz, Phys. Rev. Lett. **82**, 648 (1999).
[48] M. G. Earl and S. H. Strogatz, Phys. Rev. E **67**, 036204 (2003).
[49] L. S. Tsimring, N. F. Rulkov, M. L. Larsen, and M. Gabbay, Phys. Rev. Lett. **95**, 014101 (2005).
[50] Z. Levnajić, Phys. Rev. E **84**, 016231 (2011).
[51] H. Hong and S. H. Strogatz, Phys. Rev. Lett. **106**, 054102 (2011).